J Biol Inorg Chem (2007) 12:867–882
DOI 10.1007/s00775-007-0241-y

ORIGINAL PAPER

The Cd^{II}-binding abilities of recombinant *Quercus suber* metallothionein: bridging the gap between phytochelatins and metallothioneins

Jordi Domènech · Rubén Orihuela · Gisela Mir · Marisa Molinas · Sílvia Atrian · Mercè Capdevila

Received: 2 November 2006 / Accepted: 12 April 2007 / Published online: 15 May 2007

Abstract In this work, we have analyzed both at stoichiometric and at conformational level the Cd^{II}-binding features of a type 2 plant metallothionein (MT) (the cork oak, *Quercus suber*, QsMT). To this end four peptides, the wild-type QsMT and three constructs previously engineered to characterize its Zn^{II}- and Cu^{I}-binding behaviour, were heterologously produced in *Escherichia coli* cultures supplemented with Cd^{II}, and the corresponding complexes were purified up to homogeneity. The Cd^{II}-binding ability of these recombinant peptides was determined through the chemical, spectroscopic and spectrometric characterization of the recovered clusters. Recombinant synthesis of the four QsMT peptides in cadmium-rich media rendered complexes with a higher metal content than those obtained from zinc-supplemented cultures and, consequently, the recovered Cd^{II} species are nonisostructural to those of Zn^{II}. Also of interest is the fact that three out of the four peptides yielded recombinant preparations that included S^{2-}-containing Cd^{II} complexes as major species. Subsequently, the in vitro Zn^{II}/Cd^{II} replacement reactions were studied, as well as the in vitro acid denaturation and S^{2-} renaturation reactions. Finally, the capacity of the four peptides for preventing cadmium deleterious effects in yeast cells was tested through complementation assays. Consideration of all the results enables us to suggest a hairpin folding model for this typical type 2 plant Cd^{II}-MT complex, as well as a nonnegligible role of the spacer in the detoxification function of QsMT towards cadmium.

Keywords Cadmium–His binding · Phytochelatins · Plant metallothionein · Sulfide ligands · Yeast complementation

Electronic supplementary material The online version of this article (doi:10.1007/s00775-007-0241-y) contains supplementary material, which is available to authorized users.

J. Domènech · S. Atrian (✉)
Departament de Genètica,
Facultat de Biologia,
Universitat de Barcelona,
Av. Diagonal, 645,
08028 Barcelona, Spain
e-mail: satrian@ub.edu

R. Orihuela · M. Capdevila
Departament de Química,
Facultat de Ciències,
Universitat Autònoma de Barcelona,
08193 Bellaterra Barcelona, Spain

G. Mir · M. Molinas
Departament de Biologia,
Universitat de Girona,
Campus Montilivi,
17071 Girona, Spain

S. Atrian
Institut de Biomedicina de la Universitat de Barcelona,
Barcelona, Spain

Introduction

Cadmium is a metal that is well known for being toxic to organisms, in general, and to plants, in particular, where it causes severe metabolic malfunctions leading to intense chlorosis and growth impairment. Consequently, plants have developed efficient defence systems against cadmium toxicity, which mainly consist of chelating polypeptides that immobilize metal ions inside the cell. Two types of plant (including algae) metal-chelating peptides have been reported, enzymatically synthesized phytochelatins (PCs) and gene-encoded metallothioneins (MTs) [1]. Plant PCs, such as yeast cadystins, are polymers of glutamic acid–Cys

γ-dipeptide linked to a terminal glycine residue, the number of units in the polymer ranging from 5 to 17 [2]. They bind Cd^{II} through metal–thiolate bonds, forming Cd^{II} PC complexes of variable size [3]. These complexes typically include acid-labile sulfide ligands, also in a variable metal to sulfide to peptide ratio, which contribute to the formation of semicrystal particles known as *crystallites*, analogous to those extensively studied in yeasts [4]. *Arabidopsis* mutants lacking PC synthase have a definite cadmium-sensitive phenotype [5], and cadmium tolerance has been related to Cd^{II} PC accumulation in tobacco [6], tomatoes [7] and maize [8].

PCs were considered the only metal-defence mechanism in plants until 1980, when an MT-like peptide was first isolated in copper-treated *Agrostis* (redtop bent) roots [9], more than 20 years after the discovery of MT in animals. MTs are ubiquitous, small, Cys-rich proteins that chelate heavy-metal ions through metal–thiolate bonds. Currently, MTs have been extensively identified as a multigenic family in angiosperms (*A. thaliana* as a model [1]), in gymnosperms [10] and in algae (*Fucus*) [11], constituting family 15 of the global MT Kägi classification [12]. Plant MTs are considerably longer than their animal counterparts owing to the exclusive presence of a 30–50-residue-long, Cys-devoid region, between the N- and C-terminal Cys-rich domains (four to eight Cys each). Specifically, the distribution of the Cys residues and the length of the spacer region have been used to further classify plant MTs into four subtypes [1, 13]. Although plant MTs have been extensively related to housekeeping functions in physiological zinc and copper metabolism [14, 15] and in reactive oxygen species scavenging [1, 16, 17], early studies report that plant MT synthesis also responds to cadmium induction [17, 18]. Confirmation of the putative cadmium detoxification role of plant MTs was primarily achieved by yeast complementation studies [19]. More recently, it has been directly shown in plant cells that MTs mediate resistance and tolerance to cadmium [20, 21]. Strikingly, very little is known about the Cd^{II}-MT complexes that are formed upon plant MT synthesis in response to cadmium, mainly owing to the high level of proteolysis associated with native protein purification. Consequently and in comparison with the structural knowledge of animal MT complexes [22], there is an appalling lack of data about the interaction between heavy-metal ions and plant MTs. Unfortunately, many initial efforts in recombinant (*Escherichia coli*) plant MT synthesis did not make it possible to overcome this drawback [23, 24], and MT complexes were directly characterized as fusion proteins [25], which is of dubious biological relevance. Fortunately, this scenario is beginning to change, and the characterization of recombinant *Triticum aestivum* (wheat, [26]) and *Musa acuminata* (banana, [27]) MT complexes was recently reported.

Some time ago, we adapted our glutathione *S*-transferase based MT expression system in *E. coli*, which we have fully validated for animal MTs [28, 29], to obtain highly homogeneous preparations of undigested, full-length metal complexes from a typical dicot angiosperm MT (*Quercus suber* MT, QsMT) [30]. QsMT is a type 2 plant MT isolated in our laboratory from a cork oak (*Q. suber*) phellem complementary DNA (cDNA) library of oxidative stress induced genes. Protein expression and purification from *E. coli* cells grown in the presence of zinc, cadmium or copper enabled us to determine the Zn^{II}-, Cd^{II}- and Cu^{I}-binding properties of the full-size peptide. Our results showed that when expressed in the presence of cadmium, recombinant QsMT (rQsMT) binds a surprisingly high content of Cd^{II} in comparison with Zn^{II}, confirming that this protein could play an important role in the heavy-metal detoxification of plants [30]. Interestingly, our results also suggested the presence of acid-labile sulfide ligands in the Cd^{II}-rQsMT complexes, concordantly with the sulfide anions mediating the formation of the Cd^{II} PC crystallites. This was the first time that the participation of sulfide ligands was suspected in any MT preparation, and led to the significant discovery that, although at different ratio, all MT recombinant complexes with divalent metal ions may contain these nonproteic ligands [31]. To gain some insight into the metal cluster structure and protein folding of plant MTs we then engineered three QsMT-derived peptides: the N-terminal Cys-rich domain (N25), the C-terminal Cys-rich domain (C18) and a chimera where both Cys-rich domains were linked by a four-Gly bridge (N25-C18) instead of the original linker region of 39 amino acids (Scheme 1). Expression of these constructs in the presence of copper or zinc allowed us to analyse the binding properties for these metal ions, and to propose a protein folding model in a single metal cluster formed by the interaction of both Cys-rich domains where the linker domain, though not participating in metal coordination, is important for the stability and function of the protein [32].

In the current study, we applied the same rationale to analyse the Cd^{II}-binding features of rQsMT at stoichiometric and conformational levels. This is especially interesting owing to the participation of sulfide ions in Cd^{II}-rQsMT. Thus, the four QsMT peptides (wild-type rQsMT, N25-C18, N25 and C18) were purified from *E. coli* cells grown in the presence of cadmium, and their in vivo Cd^{II}-binding ability was determined through the chemical, spectroscopic and spectrometric characterization of the corresponding clusters. Then, the in vitro Zn^{II}/Cd^{II} replacement reactions were studied, as well as the in vitro acid denaturation and sulfide renaturation reactions. Finally, to test the capacity of the four peptides for preventing cadmium deleterious effects in yeast cells, a

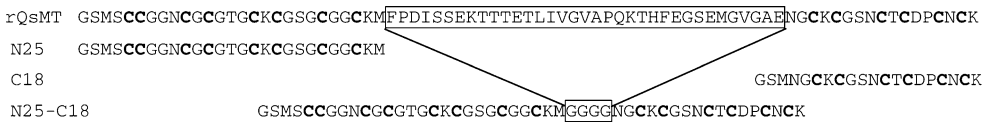

Scheme 1 Amino acid sequences of the wild-type recombinant *Quercus suber* metallothionein (*rQsMT*) and of the three deletion mutants as constructed in [32]: *N25*, the rQsMT N-terminal region, containing the first eight Cys; *C18*, the QsMT C-terminal region, containing six Cys; and *N25-C18*, the fusion of N25 and C18 through a flexible bridge of four Gly (*box*), thus devoid of the spacer region of QsMT. Additional Gly and Ser are present in the N-terminus of the four peptides owing to the recombinant synthesis strategy [28]

functional approximation was performed through yeast complementation assays. All the results enable us to suggest, for the first time, a metal-binding and folding model for a typical plant Cd^{II}-MT complex.

Materials and methods

Recombinant synthesis and purification of the Zn^{II} and Cd^{II} complexes of wild-type QsMT, N25-C18, N25 and C18

Isolation of the QsMT cDNA, construction of the N25, C18 and N25-C18 coding sequences, and cloning into the pGEX expression vector have been previously described [30, 32]. *E. coli* BL21 cells transformed with the respective recombinant plasmids pGEX-QsMT, pGEX-N25, pGEX-C18 and pGEX-N25-C18 were grown in the presence of 300 μM $ZnCl_2$ or $CdCl_2$ and hence used for recombinant syntheses. Expression and purification were performed as reported in [31], so all MT complexes were recovered in 50 mM tris(hydroxymethyl)aminomethane hydrochloride pH 7.0 solution, and were kept at –70 °C until used.

Chemical, spectroscopic and spectrometric characterization of the metal peptide complexes

Following the procedures already described by our group [31, 32], acid inductively coupled plasma atomic emission spectroscopy (ICP-AES) and amino acid analysis were used to determine the protein concentration of the different Zn^{II}- or Cd^{II}-containing preparations. Their metal-to-protein ratios were also deduced from the acid ICP-AES measurements and their mean sulfide-to-protein contents were estimated by gas chromatography–flame photometric detection (GC-FPD) [31]. The use of Na_2SO_4 as an ICP-AES standard for the Cys- and Met-derived sulfur quantification in MTs was validated by Bongers et al. [33]. However, as we reported in [31], Na_2SO_4 cannot be used as a standard for sulfide sulfur determinations as both types of sulfur enter into the plasma phase differently. Consequently, the S^{2-}-to-protein ratios cannot be obtained by direct subtraction of the acid from the conventional ICP-AES values, although both types of data are included in Tables 1 and 2. A Polyscan 61 E (Thermo Jarrell Ash) spectropolarimeter and an Alpha Plus amino acid autoanalyser (Pharmacia LKB Biotechnology) were respectively used for the ICP-AES measurements and amino acid analysis. An HP 5890 series II gas chromatograph coupled to an FPD80 CE detector (Thermo Finnigan) was employed for the GC-FPD sulfide quantifications.

The in vitro Cd^{II}-binding analyses were performed by Cd^{II} titration of the Zn^{II} peptides as described elsewhere [28], and were monitored spectroscopically and spectropolarimetrically. Electronic absorption measurements were performed using an HP-8453 diode array UV–vis spectrophotometer. A JASCO spectropolarimeter (J-715) interfaced to a computer (GRAMS/AI 7.02 software) was used for circular dichroism (CD) determinations. All manipulations involving metal ion and protein solutions were performed under an argon atmosphere, and titrations were carried out at least in duplicate to ensure reproducibility. The pH for all experiments remained constant throughout, without further addition of buffers, and the temperature was kept constant at 25 °C by means of a Peltier PTC-351S apparatus.

The molecular mass of the metal peptide species was determined by electrospray ionization (ESI) mass spectrometry (MS) performed either with a Fisons Platform II instrument (VG Biotech) controlled by MassLynx software following the same conditions previously described [32] or with an Ultima Micromass quadrupole time of flight (QTOF) instrument (ESI-QTOF), also controlled by MassLynx software and calibrated with NaI (0.2 g NaI dissolved in 100 ml of a 1:1 H_2O/2-propanol mixture). In the ESI-TOF analysis of the metallopeptides, 5 μl of the sample was injected at 40 μl/min under the following conditions: source temperature, 150 °C; desolvation temperature, 250 °C; capillary counter electrode voltage, 3.0 kV; cone potential, 80 V. Spectra were collected throughout an *m/z* range from 950 to 2,150 at a rate of 2 s per scan with an interscan delay of 0.1 s. The liquid carrier was a 10:90 mixture of acetonitrile and 5 mM ammonium acetate, pH 7. For analysis of the apo form, the samples were demetalated by acidification with HCl at pH 1.5 and MS measurements were carried out as explained for the holo forms, except that the liquid carrier was a 10:90 mixture of methanol and ammonium formate/

Table 1 Analytical characterization of the recombinant Zn^{II} complexes of *Quercus suber* metallothionein (*QsMT*) and the three QsMT-derived peptides (N25-C18, N25 and C18)

Peptide	Peptide concentration ($\times 10^{-4}$) Zn^{II}-to-peptide molar ratio			S^{2-}/peptide[c]	ESI-MS[d]			
	ICP[a]	Acid ICP[b]	Amino acid analysis		Major species	Minor species	$M_{r\ expected}$	$M_{r\ found}$
QsMT	1.3 ± 0.10	0.9 ± 0.05	0.9 ± 0.10	1.3 ± 0.40	Zn_4-QsMT		8,070.4	8,070.0 ± 0.6
	2.7 ± 0.04	3.5 ± 0.06				Zn_3-QsMT	8,007.1	8,007.4 ± 1.2
						Zn_4S_2-QsMT	8,138.6	8,138.2 ± 1.4
N25-C18	1.5 ± 0.08	1.3 ± 0.07	1.3 ± 0.11	1.0 ± 0.30	Zn_4-N25-C18		4,622.6	4,620.0 ± 0.6
	3.6 ± 0.05	3.6 ± 0.08				Zn_4S_1-N25-C18	4,656.7	4,660.2 ± 0.8
						Zn_3S_1-N25-C18	4,593.3	4,592.7 ± 0.6
N25	3.8 ± 0.12	3.2 ± 0.08	3.2 ± 0.23	0.3 ± 0.10	Zn_2-N25		2,535.6	2,534.0 ± 0.5
	2.0 ± 0.09	2.2 ± 0.10				Zn_3-N25	2,599.0	2,600.5 ± 0.7
						Zn_7S_1-$(N25)_2$	5,295.4	5,295.5 ± 0.7
C18	3.5 ± 0.11	3.4 ± 0.09	3.3 ± 0.38	0.0 ± 0.00	Zn_2-C18		2,152.1	2,150.0 ± 0.7
	1.9 ± 0.10	1.8 ± 0.08				Zn_1-C18	2,088.7	2,086.4 ± 0.8
						Zn_5-$(C18)_2$	4,367.6	4,367.8 ± 1.9

ICP inductively coupled plasma, *ESI-MS* electrospray ionization mass spectrometry

[a] Peptide concentration and $Zn^{II}$to-peptide ratio calculated from conventional ICP atomic emission spectroscopy (AES) results

[b] Peptide concentration and Zn^{II}-to-peptide ratio calculated from acid ICP-AES results

[c] S^{2-}-to-peptide ratio measured by gas chromatography–flame photometric detection (GC-FPD)

[d] Experimental and theoretical molecular weights corresponding to the Zn^{II} peptides. Zn^{II} contents were calculated from the mass difference between holo and apo proteins

Table 2 Analytical characterization of the recombinant Cd^{II} complexes of QsMT and the three QsMT-derived peptides (N25-C18, N25 and C18)

Peptide	Peptide concentration ($\times 10^{-4}$ M) Cd^{II}-to-peptide molar ratio			S^{2-}/peptide[c]	ESI-MS[d]			
	ICP[a]	Acid ICP[b]	Amino acid analysis		Major species	Minor species	$M_{r\ expected}$	$M_{r\ found}$
QsMT(1)	1.5 ± 0.20	0.8 ± 0.03	0.8 ± 0.11	2.9 ± 0.80	Cd_6S_4-QsMT		8,615.5	8,617.2 ± 0.3
	2.9 ± 0.07	6.7 ± 0.05				Cd_7S_4-QsMT	8,725.9	8,723.7 ± 1.1
QsMT(2)	1.5 ± 0.22	0.6 ± 0.05	0.6 ± 0.09	2.4 ± 0.60	Cd_6S_4-QsMT		8,615.5	8,619.1 ± 0.8
	2.5 ± 0.08	6.3 ± 0.08				Cd_7S_4-QsMT	8,725.9	8,726.0 ± 0.7
QsMT(3)	2.3 ± 0.31	1.3 ± 0.07	1.3 ± 0.18	2.2 ± 0.70	Cd_5-QsMT		8,368.8	8,370.1 ± 0.6
	3.7 ± 0.10	5.3 ± 0.08				Cd_6S_4-QsMT	8,615.5	8,618.2 ± 1.2
N25-C18	2.4 ± 0.26	1.0 ± 0.04	1.0 ± 0.20	2.4 ± 0.60	Cd_6S_4-N25-C18		5,167.7	5,169.6 ± 0.5
	2.4 ± 0.09	5.9 ± 0.07				Cd_5-N25-C18	4,921.1	4,922.1 ± 0.2
N25	3.0 ± 0.35	1.2 ± 0.04	1.2 ± 0.21	2.8 ± 0.60	Cd_7S_4-$(N25)_2$		5,726.8	5,730.5 ± 1.9
	1.4 ± 0.13	3.8 ± 0.09				Cd_6-$(N25)_2$	5,480.1	5,478.7 ± 2.0
C18	2.9 ± 0.12	2.8 ± 0.10	2.7 ± 0.30	0.5 ± 0.40	Cd_4-$(C18)_2$		4,492.3	4,490.9 ± 0.6
	2.1 ± 0.12	2.3 ± 0.10				Cd_5-$(C18)_2$	4,602.7	4,600.9 ± 1.2

[a] Peptide concentration and Cd^{II}-to-peptide ratio calculated from conventional ICP-AES results

[b] Peptide concentration and Cd^{II}-to-peptide ratio calculated from acid ICP-AES results

[c] S^{2-}-to-peptide ratio measured by GC-FPD

[d] Experimental and theoretical molecular weights corresponding to the Cd^{II} peptides. Cd^{II} contents were calculated from the mass difference between holo and apo proteins

ammonia at pH 1.5. In all cases, the theoretical molecular masses were calculated according to [32] except for the sulfide-containing species, where two additional protons were added per sulfide anion.

Demetalation and reconstitution of the Cd^{II} complexes of rQsMT and the three derived peptides

Two different strategies were used for the demetalation of the MT complexes in this work: acidification and EDTA treatment. For acidification, and according to equivalent experiments with Cd^{II} PC complexes [34], the four Cd^{II} peptide preparations were acidified from neutral pH to a pH lower than 1 with 1–10^{-3} M HCl depending on the stage of the titration, and were reneutralized afterwards to pH 7.0 with 1–10^{-3} M NaOH, also depending on the stage of the titration. After reneutralization, several molar equivalents of a standard solution of Na_2S prepared as described in [31] were added. All the CD and UV–vis changes experienced by the samples during these pH variations and sulfide additions were recorded and corrected for dilution effects. When possible, ESI-MS analyses of the intermediate and resulting final solutions were also performed.

According to procedures reported in the literature [35], a 16 μM solution of Cd^{II}-rQsMT at pH 7.5 was treated with 10–50 mM EDTA, depending on the stage of the titration, and the spectropolarimetric changes were recorded.

Yeast functional complementation assays

Following the details reported in [32], two MT-deficient, copper-sensitive *Saccharomyces cerevisiae* strains were used, *cup1*^{S}: DTY3 (*MATa*, *leu2-3*, *112his3*$^\Delta$*1*, *trp1-1*, *ura3-50*, *gal1 CUP1*^{S}), harbouring only one copy of the *CUP1* MT gene; and *cup1*$^\Delta$: DTY4 (same with *cup1::URA3*), thus with no copy of *CUP1* [36]. The growth of yeast cells transformed with the plasmids p424-QsMT, p424-N25-C18, p424-N25 or p424-C18, constructed as previously described [30, 32, 37], was assayed in culture media supplemented with or without $CdCl_2$ (1.5, 2.5 or 3.5 μM for the plate).

Results and discussion

The metal complexes rendered by the three QsMT-derived peptides (N25-C18, N25 and C18) when biosynthesized in zinc- or cadmium-enriched media were analysed and characterized by spectroscopic and spectrometric methods, and the data were compared with those of the full-length rQsMT [30, 32]. Independently of the metal ions supplemented in the media, acidification to pH 1.0 of each recombinant peptide yielded single apo forms whose molecular masses were in accordance with the values calculated from their amino acid composition [32], this confirming their identity and integrity. None of the CD spectra of the four demetalated peptides exhibited absorptions in the 220–400-nm range, which is especially significant in the case of apo-QsMT, as this indicates that the aromatic residues of the spacer region are CD-silent. However, the UV–vis spectrum of apo-QsMT showed absorptions in the range 260–280 nm (Fig. 3j) attributable to the two Phe residues of the spacer.

The Zn^{II}-binding features of rQsMT and derived peptides: a deeper insight

The in vitro Zn^{II}/Cd^{II} replacement studies of the four recombinant peptides required biosynthesis and analytical characterization of the corresponding Zn^{II} complexes, previously characterized in [32]. However, our current knowledge of the presence of sulfide ligands in the recombinant MT species [31] together with the use of ESI-QTOF allowed refining of our previous data [32], particularly their metal and S^{2-} contents (Table 1). The present results revealed that Zn^{II}-C18 was the only case where S^{2-} ligands were not detected by GC-FPD. In contrast, rQsMT, N25-C18 and N25 gave rise to minor S^{2-}-containing species. It should be noted that, as already reported in [31], we have found that GC-FPD always overestimates the S^{2-} content of the MT samples. Consequently, there is a discordance between the S^{2-}/protein quantification achieved by GC-FPD and the stoichiometries and relative abundances of the MT species detected by ESI-MS.

Analysis of the Cd^{II}-binding features of rQsMT

Multiple recombinant syntheses of the full-length QsMT in cadmium-rich medium yielded three kinds of in vivo preparations, namely rQsMT types 1, 2 and 3, which could not be related to specific culture conditions. According to the MS data shown in Table 2, Cd^{II}-rQsMT(1) and Cd^{II}-rQsMT(2) showed identical speciation: Cd_6S_4 and Cd_7S_4 as the most abundant species, while Cd^{II}-rQsMT(3) yielded major Cd_5 and minor Cd_6S_4 complexes. Therefore, the unknown ligand of [30] could be readily identified as four S^{2-} anions. In any case, none of the Cd^{II}-rQsMT complexes were either isostoichiometric or isostructural to their Zn^{II}-rQsMT counterpart. Although all Cd^{II}-rQsMT types consisted of Cd^{II} homometallic samples of close speciation, their CD fingerprints were markedly dissimilar (Fig. 1a). Interestingly, these CD features were exchangeable by in vitro acidification or demetalation treatments, as explained further below.

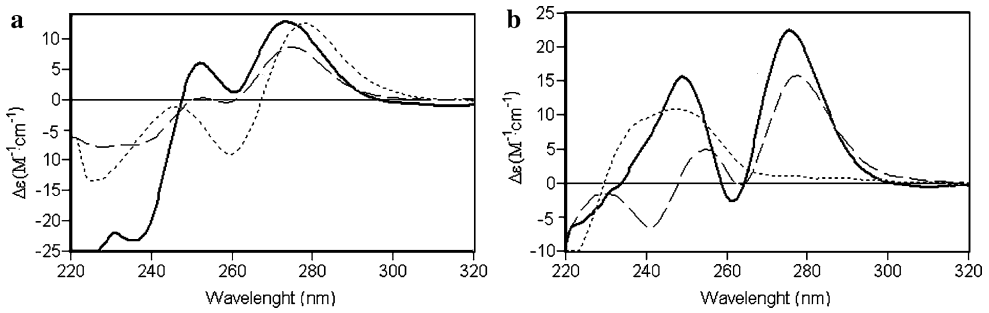

Fig. 1 Comparison of the normalized circular dichroism (CD) spectra of the following recombinant metallothionein (MT) preparations: **a** Cd^{II}-rQsMT(1) (*dotted line*), Cd^{II}-rQsMT(2) (*dashed line*), Cd^{II}-rQsMT(3) (*solid line*) **b** Cd^{II}-N25-C18 (*solid line*), Cd^{II}-N25 (*dashed line*), Cd^{II}-C18 (*dotted line*). *rQsMT* recombinant *Quercus suber* MT

Overall analysis of the in vitro Zn^{II}/Cd^{II} replacement in Zn^{II}-rQsMT led us to propose Cd_4-QsMT (major), Cd_5-QsMT, and several minor S^{2-}-containing complexes of close metal stoichiometry, as the final products of this reaction, even in the presence of excess Cd^{II} (whole spectroscopic and spectrometric data included in Fig. 2, Table S1). These species were similar to those of the Cd^{II}-rQsMT(3) preparation, but were absent in Cd^{II}-rQsMT(1) and Cd^{II}-rQsMT(2) samples (Table 2). Notably, none of the CD fingerprints of the three Cd^{II}-rQsMT types were reproduced during the Cd^{II} titration (Figs. 1a, 2a, b). As the main difference between the in vivo and in vitro Cd^{II}-binding abilities of QsMT was the presence of S^{2-}-rich Cd_6S_4-rQsMT complexes (in the in vivo samples), we extended the Cd^{II} titration by gradually adding Na_2S after 7 equiv Cd^{II} had been added to Zn^{II}-rQsMT. This gave rise to an absorption increase in the 260–320-nm region (Fig. 2c, d, g, h, k, l), in accordance with the S^{2-} anions being incorporated into the Cd^{II} complexes [34]. The final CD fingerprints (Fig. 2d) clearly evolved towards the envelopes recorded for Cd^{II}-rQsMT (Fig. 1a). Despite the drawbacks associated with generation of Na^+ adducts, ESI-MS analysis of the final samples revealed the presence of S^{2-}-containing species with higher nuclearity than those present before Na_2S addition (i.e. Cd_7S_9-QsMT and Cd_6S_6-QsMT, Table S1). All these data reinforce the hypothesis of S^{2-} as a determinant of (1) the nuclearity of Cd^{II}-rQsMT complexes and (2) the differences between the biosynthesized Cd^{II}-rQsMT samples and the in vitro constituted Cd^{II}-QsMT complexes.

Finally, acidification/reneutralization of the three Cd^{II}-rQsMT preparation types shed light on their different nature. Acidification of Cd^{II}-rQsMT(3) from pH 7 to 4.5 caused a decrease in the intensity of the CD shoulder at approximately 250 nm, to give rise to a CD profile very similar to that of Cd^{II}-rQsMT(1) (whose CD spectrum remains invariable between pH 7.0 and 4.3, Fig. S1), with one intermediate step corresponding to the CD of Cd^{II}-rQsMT(2) (Fig. 3a). Thus, at pH 4.5 any of the three Cd^{II}-rQsMT types exhibited the same CD spectrum [i.e. that of Cd^{II}-rQsMT(1)], which remained unaltered between pH 4.5 and 3.5 (Fig. 3b), to render at pH 1 the typical CD and UV spectra of an apo-MT with aromatic amino acids (Fig. 3c, d, i, j). The H_2S odour was perceptible during the three acidifications, confirming the acid-labile character of the S^{2-} ligands of the original complexes. Reneutralization up to pH 7 of the resulting S^{2-}-devoid samples (Fig. 3e, k, q) gave rise to Cd_4-QsMT (major) and Cd_5-QsMT (minor) species (ESI-MS data not shown) whose CD envelopes evidently did not reproduce those of any of the Cd^{II}-rQsMT preparations. As before, addition of Na_2S to these solutions caused dramatic changes to their spectroscopic features (Fig. 3f, l, r) and rendered S^{2-}-containing complexes (Cd_8S_6 and Cd_7S_2) whose CD fingerprint resembled that of Cd^{II}-rQsMT(3) (Fig. 4a). Interestingly, during the demetalation of Cd^{II}-rQsMT(1) by EDTA (Fig. 4b, c), the addition of the first EDTA equivalent (Fig. 4b) increased chirality at approximately 280 nm, while not altering that at approximately 250 nm. Afterwards, increasing molar ratios of EDTA led to samples showing CD spectra similar to that of Cd^{II}-rQsMT(3) (Fig. 4c).

The comprehensive consideration of all these data suggests that the heterogeneity of the Cd^{II}-rQsMT samples (types 1–3) was due to two main factors: (1) the already mentioned relative abundance of S^{2-}-containing complexes in the sample and (2) the putative participation of the His of the spacer in cadmium coordination, as suggested by the following hints. First, preliminary Raman data revealed the presence of metal–His bonds in the Cd^{II}-rQsMT complexes, and their absence in Zn^{II}-rQsMT [38]. Second, literature data suggest that CD shoulders at approximately 250 nm can be attributed to Cd^{II}–His coordination [39, 40], which we have corroborated with studies in mammalian MT1 mutants [41] and chicken MT [42]. And third, a differential His participation in Cd^{II} binding would be consistent with the

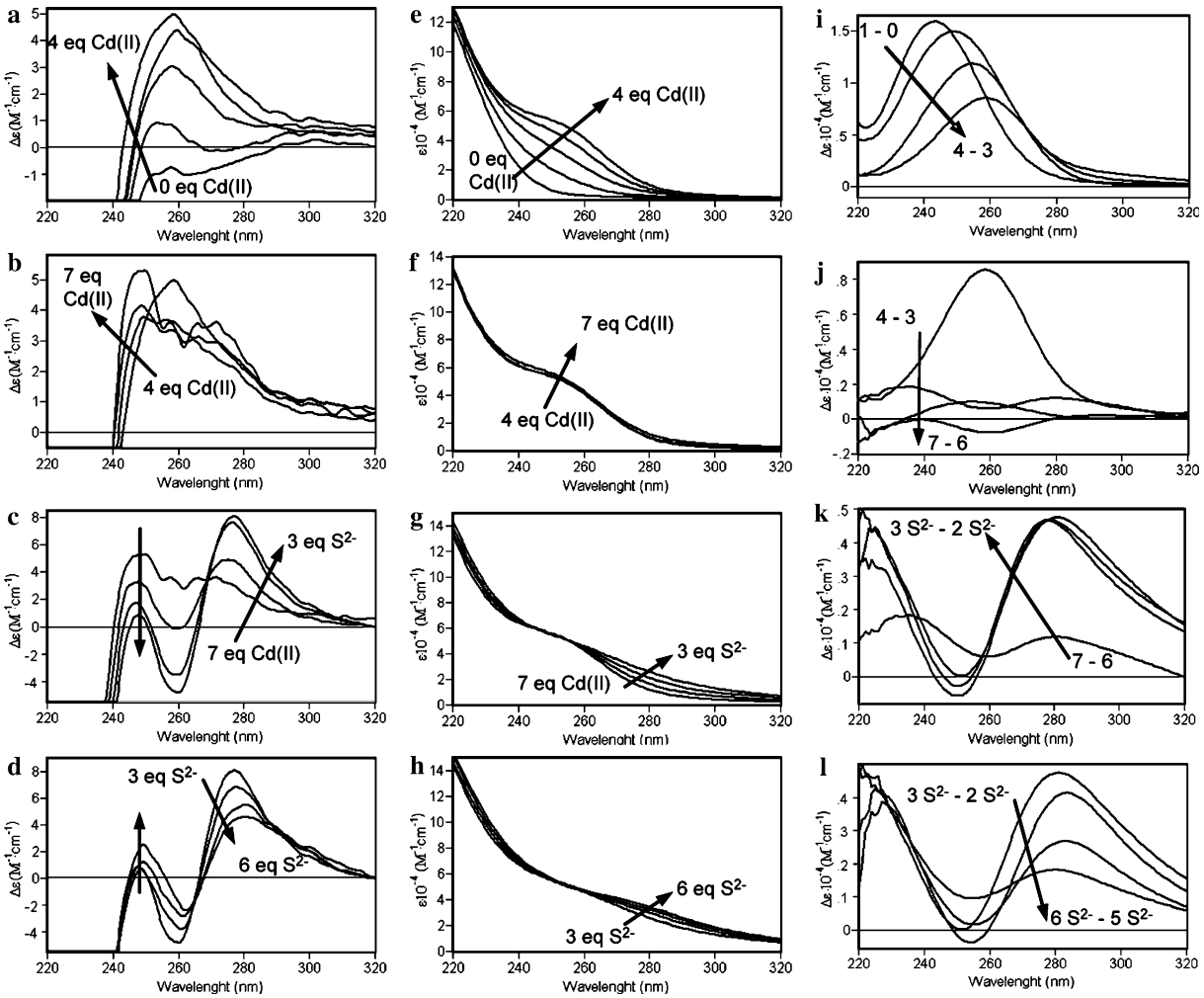

Fig. 2 CD (**a**–**d**), UV–vis (**e**–**h**) and UV–vis difference (**i**–**l**) spectra corresponding to the titration of a 20 μM solution of Zn-rQsMT with Cd(II) at pH 7.0 followed by the addition of several equivalents of Na_2S. *Arrows* show the evolution of the spectra when the indicated number of Cd(II) or S^{2-} equivalents were added

initially different CD spectra of the three types of Cd^{II}-rQsMT converging to an identical CD fingerprint at pH 4.5, after His protonation. Finally, the EDTA-induced Cd^{II} displacement from the rQsMT complexes could cause conformational rearrangements allowing His participation in Cd^{II} coordination. This hypothesis is highly consistent with the fact that the lower the Cd^{II} content, the higher the chirality at approximately 250 nm [cf. rQsMT(3), Table 2, Fig. 1a].

Thus, all our data are in concordance with rQsMT(3) being mainly composed of S^{2-}-devoid Cd_5 complexes where His may participate in cadmium coordination; rQsMT(1) containing S^{2-}-rich Cd_6 and Cd_7 complexes with no His participation; and rQsMT(2) being a mixture of rQsMT(1) and rQsMT(3). Therefore, when Cd^{II}-rQsMT is synthesized in *E. coli*, and depending on the folding that the protein adopts when binding the Cd^{II} ions, the His residue of the spacer may or may not participate in Cd^{II} binding, with this determining the stoichiometry and the conformation of the final complexes.

Analysis of the Cd^{II}-binding features of N25-C18

N25-C18 synthesized in cadmium-rich medium yielded homometallic Cd^{II} complexes, among which Cd_6S_4-N25-C18 and Cd_5-N25-C18 were the most abundant species (Table 2). Thus, the Cd^{II}-N25-C18 complexes were neither isostoichiometric nor isostructural to their Zn^{II}-N25-C18 counterparts, as neither were the rQsMT species. Cd^{II}-N25-C18 showed a characteristic CD spectrum composed of two Gaussian bands centred at approximately 250 (Cd^{II} thiolate) and 280 nm (Cd^{II} sulfide) chromophores (Fig. 1b), which was clearly different from those of the diverse Cd^{II}-rQsMT types (Fig. 1).

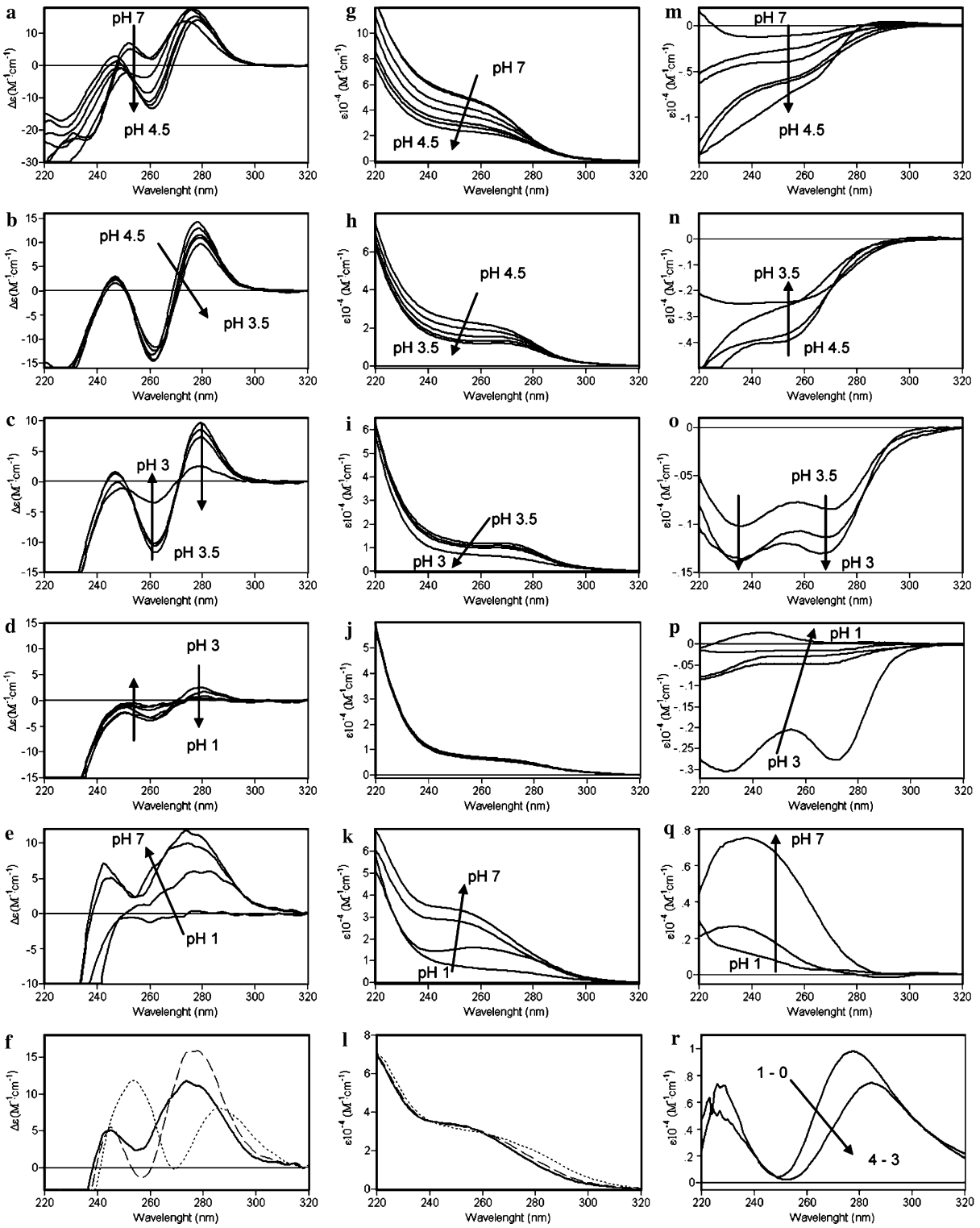

Fig. 3 CD (**a**–**f**), UV–vis (**g**–**l**) and UV–vis difference (**m**–**r**) spectra corresponding to the acidification (**a**–**d**, **g**–**j**, **m**–**p**) and reneutralization (**e**, **k**, **q**) of a 20 μM solution of Cd^{II}-rQsMT(3); and addition of several Na_2S equivalents (**f**, **l**, **r**) to the final reneutralized solution. *Arrows* show the evolution of the spectra during acidification and reneutralization processes. *Curves* in **f**, **l** and **r** correspond to the reneutralized Cd^{II}-QsMT solution of **e** (*solid line*) and those recorded after addition of 1 equiv (*dashed line*) and 4 equiv (*dotted line*) S^{2-} to the former

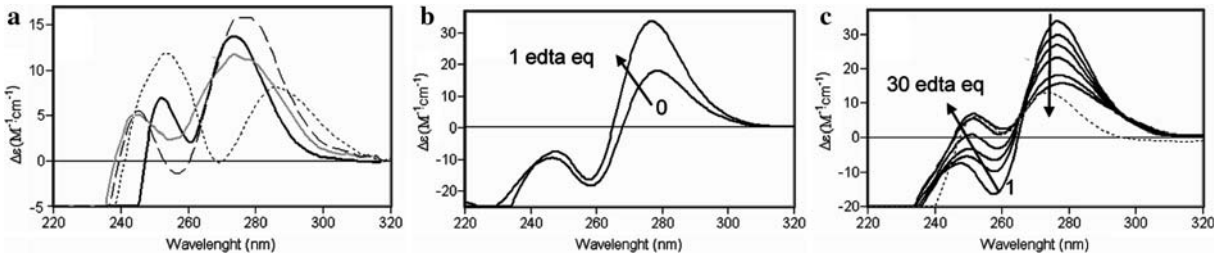

Fig. 4 **a** Comparison of the CD spectra of Cd^{II}-rQsMT(3) (*solid black line*), the acidified/reneutralized Cd^{II}-QsMT sample (*solid grey line*) and with addition of 1 equiv (*dashed line*) and 4 equiv (*dotted line*) S^{2-} to the previous sample. **b**, **c** CD spectra corresponding to the addition of the first EDTA equivalent and of 1, 1.5, 2, 3, 9 and 30 equiv EDTA to a 16 μM Cd^{II}-rQsMT(1) sample. The *dotted line* in **c** corresponds to the CD spectrum of the Cd^{II}-rQsMT(3) preparation. *Arrows* show the evolution of the spectra during the demetalation process

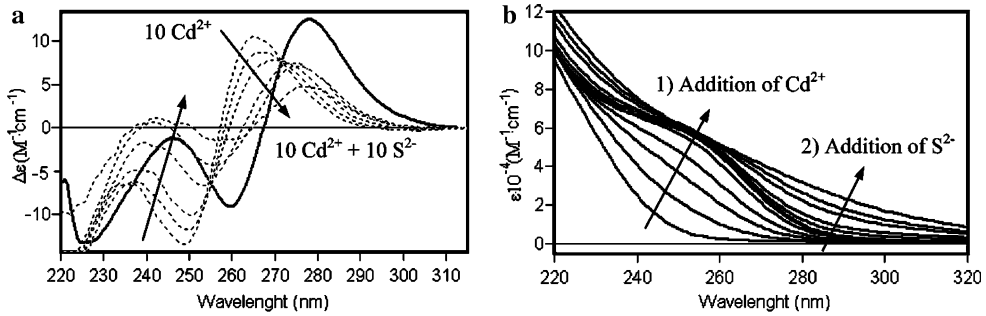

Fig. 5 **a** Comparison between the CD spectra of Cd^{II}-rQsMT(1) (*solid line*) and those recorded after the addition of 1, 2, 5, 7 and 10 equiv Na_2S at the end of the titration of Zn^{II}-N25-C18 with Cd(II), i.e. after 10 equiv Cd^{II}. **b** UV–vis spectra recorded during the addition of 1–10 equiv Cd^{II} to Zn_4-N25-C18, leading to the formation of Cd_5-N25-C18, followed by the addition of 1, 2, 5, 7 and 10 equiv Na_2S. The difference in CD intensities between Cd^{II}-rQsMT(1) and the final Cd^{II}-N25-C18 sample and the deviations of the baseline of the UV–vis spectra are due to the turbulence of the final stages of Na_2S additions, caused by precipitation of the excess Cd^{II} as CdS

Titration of Zn_4-N25-C18 with Cd^{II} (full data in Fig. S2, Table S2) rendered Cd_5-N25-C18 as the major species even for an excess of Cd^{II} and resulted in a different CD spectrum from that of the in vivo sample. Surprisingly, although blueshifted it resembled that of Cd^{II}-rQsMT(1) (Fig. 5a). Addition of Na_2S after the final titration step further increased this resemblance, with a clear indication of S^{2-} Cd^{II} coordination (Fig. 5). These results are fully consistent with the previous hypothesis about the Cd^{II}-coordinating behaviour of His in rQsMT. Hence, N25-C18 that is devoid of this residue can reproduce the features of Cd^{II}-rQsMT(1), where we presume no Cd^{II}–His contributions, and never those of rQsMT(3).

It is especially worth noting that titration of Zn^{II}-N25-C18 with Cd^{II} and S^{2-} yielded complexes more similar to Cd^{II}-rQsMT than to Cd^{II}-N25-C18. However, a process of acidification/reneutralization/S^{2-} addition of the biosynthesized Cd^{II}-N25-C18 ended up with a CD fingerprint very similar to the initial one (Fig. S3). The interpretation of the spectroscopic data of these reactions was more straightforward than for Cd^{II}-rQsMT owing to the absence of His and Phe in the N25-C18 polypeptide. Thus, it could be deduced that acidification of Cd_6S_4-N25-C18 from pH 7 to 4.5 promoted an important structural rearrangement. The 250-nm Gaussian band became a derivative-shaped band at the same wavelength, so some Cd^{II} thiolate chromophores could be lost, while S^{2-} would remain bound to the Cd^{II} ions. We cannot discard the migration of some thiolate-bound Cd^{II} to S^{2-}-rich environments, as suggested by the UV–vis difference spectra in Fig. S3c. It was not until pH between 4 and 2 that CD absorptions at approximately 280 nm—together with those remaining at approximately 250 nm—disappeared, to generate a characteristic apo-MT spectrum. At this point, a strong H_2S odour was perceptible and the Cd^{II} ions released to the solution visibly precipitated as CdS. In spite of the turbidity of the sample, it was reneutralized to pH 7. Reincorporation of the Cd^{II} ions to N25-C18 gave rise to an intense and very wide CD signal centred at approximately 260 nm and that was very different from that of the initial in vivo Cd^{II}-N25-C18 (Fig. 6a), as expected from the loss of most of the S^{2-} ligands. This new CD fingerprint could be interpreted as being composed of one absorption centred at about 250 nm—attributable to $Cd^{II}(SCys)_4$— and other absorp-

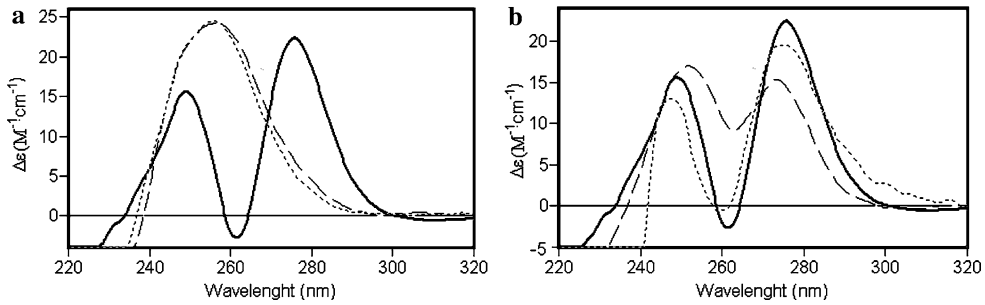

Fig. 6 **a** Comparison between the normalized CD spectra of recombinant Cd^{II}-N25-C18 (*solid line*), Zn^{II}-N25-C18 after the addition of 3 equiv Cd^{II} (*dotted line*) and the reneutralized Cd^{II}-N25-C18 sample (*dashed line*). **b** Comparison between the CD spectra of recombinant Cd^{II}-N25-C18 (*solid line*), the reneutralized Cd^{II}-N25-C18 sample after the addition of 4 equiv S^{2-} (*dashed line*) and the reneutralized Cd^{II}-QsMT sample after the addition of 1 equiv S^{2-} (*dotted line*)

tions in the 270–320-nm range—due to Cd^{II}-S^{2-} if it is assumed that some CdS particles became trapped by some Cys residues. Although this may appear speculative, it is consistent with the observations that (1) the envelope of the CD spectrum of the reneutralized sample perfectly matched that recorded for the addition of 3 equiv Cd^{II} to Zn_4-N25-C18 (Fig. 6a), a preparation that contained one S^{2-} per MT (Table 1), and (2) that the tail of the CD absorptions extending until 300 nm could only be attributed to Cd^{II}–S^{2-} chromophores. Subsequent Na_2S addition to the reneutralized sample caused dramatic changes in the CD spectra already from the first step (Fig. 6b) to practically reproduce, for 3–4 equiv S^{2-} added, the spectrum of the initial in vivo Cd^{II}-N25-C18. This final CD profile was not too different from that achieved by Cd^{II}-rQsMT(1) after a similar acidification/reneutralization/S^{2-} addition process (Fig. 6b), which indicates that both polypeptides can, depending on the conditions, show similar Cd^{II}-binding behaviour when His does not contribute to Cd^{II} coordination.

Analysis of the Cd^{II}-binding features of the separate N25 and C18 peptides

The syntheses of the separate N25 and C18 peptides in cadmium-rich media yielded dimeric Cd^{II} homometallic complexes (Table 2). Cd_7S_4-$(N25)_2$ and Cd_6-$(N25)_2$ were the main species of a Cd^{II}-N25 preparation exhibiting high sulfide content (2.8 S^{2-} per peptide). Conversely, Cd^{II}-C18 was mainly composed of major Cd_4-$(C18)_2$ and minor Cd_5-$(C18)_2$ complexes (Fig. 7), in concordance with the very low S^{2-} content detected by GC-FPD (0.5 S^{2-} per peptide). The CD spectra of these samples (Fig. 1b) also reflected their differential S^{2-} content, since Cd^{II}-N25, unlike Cd^{II}-C18, gave rise to CD absorptions at approximately 280 nm.

The in vitro Zn^{II}/Cd^{II} replacement followed by S^{2-} addition, and the acidification/reneutralization/S^{2-} addition studies were also undertaken for the separate N25 and C18 peptides (results summarized in Fig. 8, and full data included in Figs. S4–S7, Tables S3, S4). In vivo Cd^{II}-N25 aggregates could not be reproduced in vitro by any of the methods assayed. Starting from major monomeric Zn_2-N25 species with a very low S^{2-} content, the dimeric Cd_7S_4-$(N25)_2$ complexes could hardly be obtained, considering that species with a maximum of three Cd^{II} ions were obtained at the end of the titration. Remarkably, acidification and reneutralization of in vivo Cd_7S_4-$(N25)_2$ did not lead to the original complexes. However, the addition of Na_2S either at the end of the Cd^{II} titration or after reneutralization gave rise to CD envelopes that practically coincided with that obtained for the acidification at pH 4 of in vivo Cd^{II}-N25 (Fig. 8a). This suggests that N25 is unable to achieve in vitro the same folding as in in vivo conditions, which basically implies dimerization and participation of S^{2-} ligands.

In a completely different scenario, the monomeric Zn_2-C18 complexes, where S^{2-} was not detected by GC-FPD, easily rendered, after addition of 2 equiv Cd^{II}, Cd_4-$(C18)_2$ dimers that exactly reproduced the CD fingerprint of the in vivo Cd^{II}-C18 preparation (Fig. 8b). As acidification and reneutralization of the in vivo Cd^{II}-C18 sample required just a small amount of Na_2S to regenerate the initial CD envelope, it is sensible to assume the presence of minute amounts of S^{2-} in Zn^{II}-C18, enough to yield in vitro the S^{2-}-containing Cd^{II}-C18 complexes.

Finally, the Cd^{II} titration of an equimolar mixture of Zn^{II}-N25 and Cd^{II}-C18, hereafter referred to as cotitration, was performed to analyse possible interactions between the separate N25 and C18 peptides (Fig. 9, Table S5). The CD spectrum of the initial mixture perfectly matched the sum of the spectra of both separated Zn^{II} complexes (Fig. 10a), which suggests that they do not interact in solution. As this CD fingerprint was clearly different from that of Zn^{II}-N25-C18, a dumbbell fold for this chimeric Zn^{II} peptide could already be ruled out. The Zn^{II}-N25 plus Zn^{II}-C18 mixture (Fig. 9) saturated for 7 equiv Cd(II) added, yielding a CD

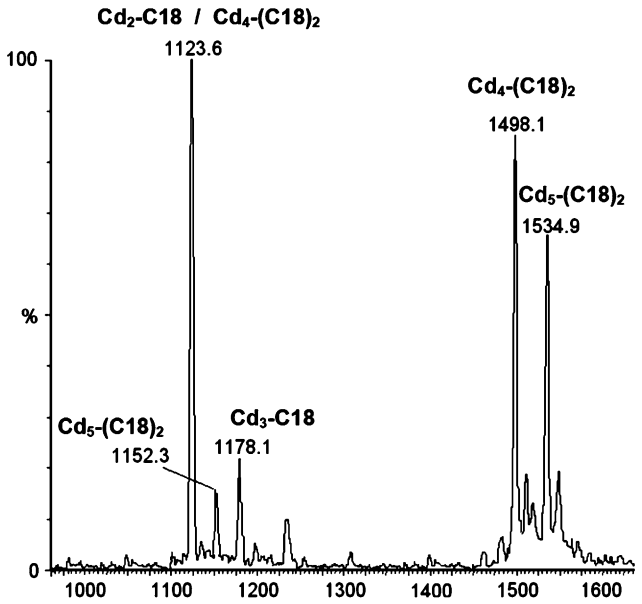

Species	$MW_{theoretical}$	(M+2)/2	(M+3)/3	(M+4)/4
Cd_2-C18	2246.14	**1124.1**	749.7	562.5
Cd_3-C18	2356.55	**1179.3**	786.5	590.1
Cd_4-$(C18)_2$	4492.28	2247.1	**1498.4**	**1124.1**
Cd_5-$(C18)_2$	4602.69	2302.3	**1535.2**	**1151.7**

Fig. 7 Electrospray ionization (ESI) mass spectrometry (MS) spectrum of the recombinant Cd^{II}-C18 preparation with indication of the theoretical molecular weights of the Cd^{II}-C18 species and the MS peaks expected for each charge state. The assessment of the presence of C18 dimers was made on the basis of a deconvolution method [32] allowing us to identify two types of ESI-MS peaks corresponding to dimeric forms: (1) peaks that match the *m*/*z* charge states of a $(Cd_n$-$MT)_2$ form (*z* being an odd value); (2) peaks that only match the molecular weight of two peptide chains binding an odd number of Cd^{II} ions. Furthermore, some peaks could be either interpreted as corresponding to a monomer of *m*/*z* or to a dimer of 2*m*/2*z* ratio

fingerprint (Fig. 10b) practically coincident with the sum of the final spectra of the separate Cd^{II} titrations of Zn^{II}-N25 and Zn^{II}-C18. In these reactions, major Cd_3-N25 and Cd_4-$(C18)_2$ complexes were respectively formed; the same species that were detected as major products of the cotitration (ESI-MS analysis in Table S5). Thus, both separate peptides behaved equally when titrated alone or in each other's presence: N25 evolving from monomeric Zn_2 to monomeric Cd_3 species, and C18 from monomeric Zn_2 to dimeric Cd_4 complexes. The difference between the final CD fingerprint of the cotitration and those of the in vivo Cd^{II}-N25-C18 (Fig. 10b) or those reached at the end of the Zn^{II}-N25-C18 titration with Cd^{II} (Fig. S2) implies a dependent behaviour of both regions in the N25-C18 polypeptide when coordinating Cd^{II}. It is worth noting that heterodimers (N25/C18) were also detected at the end of the cotitration, although as minor species (Table S5), which is highly significant in order to support a hairpin model for Cd^{II}-N25-C18 (discussed later). The small amount of heterodimers is consistent with the low peptide concentration at which the cotitration was performed to allow monitoring by CD, and with the fact that N25 seems not to require interaction with other peptides (same N25 or C18) to form Cd^{II} complexes in solution.

QsMT cadmium detoxification capacity in yeast

To test whether the QsMT-derived peptides provided protection against cadmium toxicity, and to what extent, N25, C18 or N25-C18 were expressed in *CUP1*-deficient yeast cells ($cup1^{\Delta}$). Cells transformed with the nonrecombinant plasmid or cells synthesizing the full-length QsMT were used as negative and positive controls, respectively. In the absence of supplemented cadmium, all the strains yielded colonies of similar size (Fig. 11a), this showing that the presence of the QsMT peptides had no inherent effect on growth. Phenotype recovery was then evaluated in terms of capacity for growing in the presence of cadmium. Control p424 $cup1^{\Delta}$ cells were sensitive to Cd^{II} concentrations as low as 1.5 μM, whereas the same cells synthesizing QsMT were able to grow at a similar rate as $cup1^{S}$ at 1.5 μM Cd^{II},

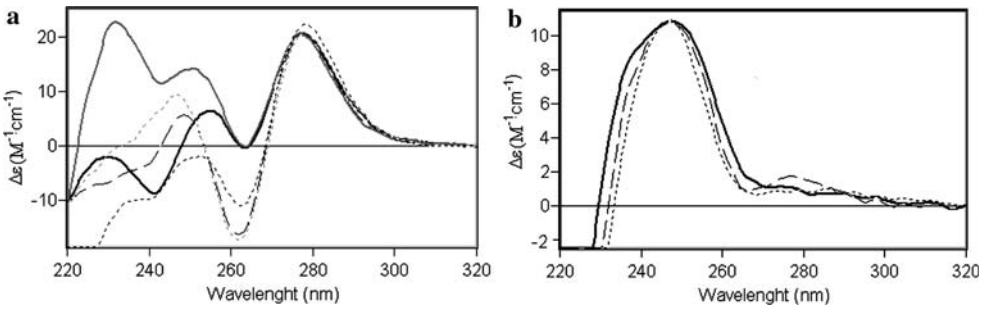

Fig. 8 **a** Comparison between the normalized CD spectra of recombinant Cd^{II}-N25 (*solid black line*), Zn^{II}-N25 after the addition of 9 equiv Cd^{II} (*solid grey line*), Zn^{II}-N25 after the addition of 10 equiv Cd^{II} and 4 equiv S^{2-} (*dotted grey line*), the Cd^{II}-N25 sample acidified to pH 4 (*dashed black line*) and the reneutralized Cd^{II}-N25 sample after the addition of 1 equiv S^{2-} (*dotted black line*). **b** Comparison between the CD spectra of recombinant Cd^{II}-C18 (*solid black line*), the reneutralized Cd^{II}-C18 sample after the addition of 2 equiv S^{2-} (*dashed line*) and the Zn^{II}-C18 sample after the addition of 2 equiv Cd^{II} (*dotted line*)

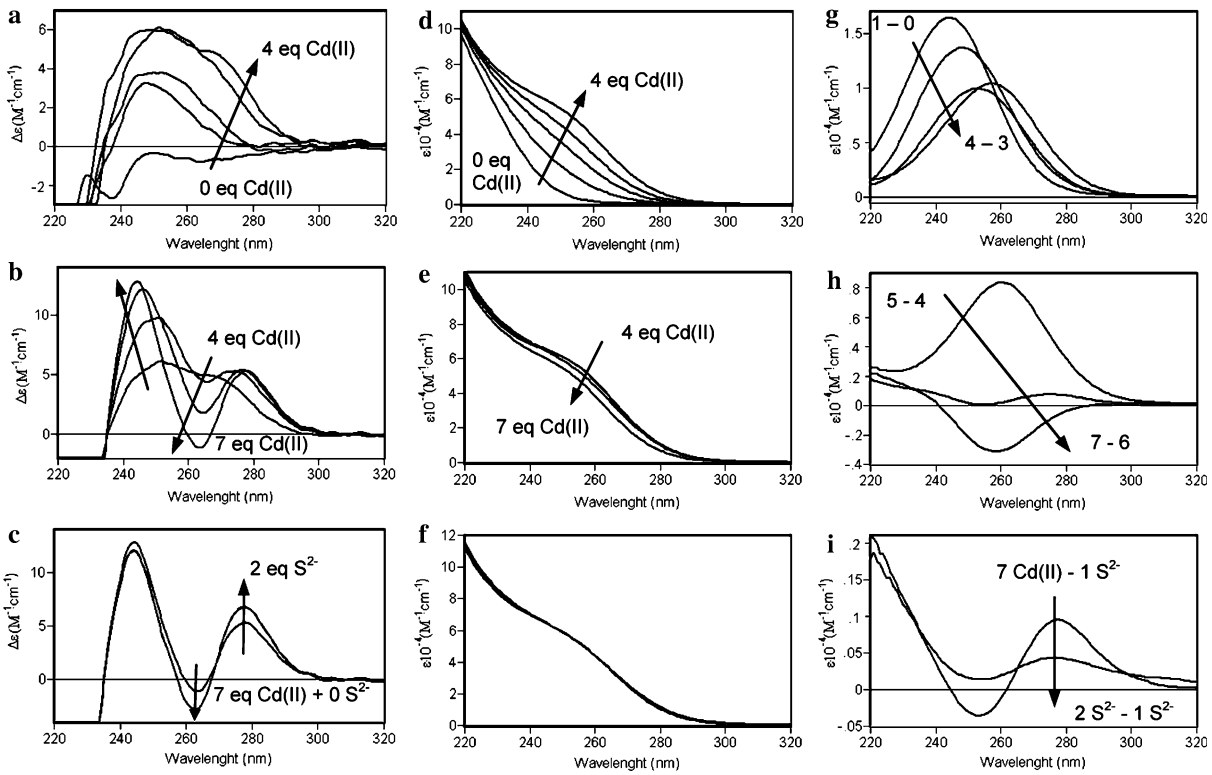

Fig. 9 CD (**a**–**c**), UV–vis (**d**–**f**) and UV–vis difference (**g**–**i**) spectra corresponding to the titration of a solution of 20 μM Zn^{II}-N25 and 20 μM Zn^{II}-C18 with Cd^{II} at pH 7.0 followed by the addition of 1 and 2 equiv Na_2S. *Arrows* show the evolution of the spectra when the indicated number of Cd^{II} or S^{2-} equivalents were added

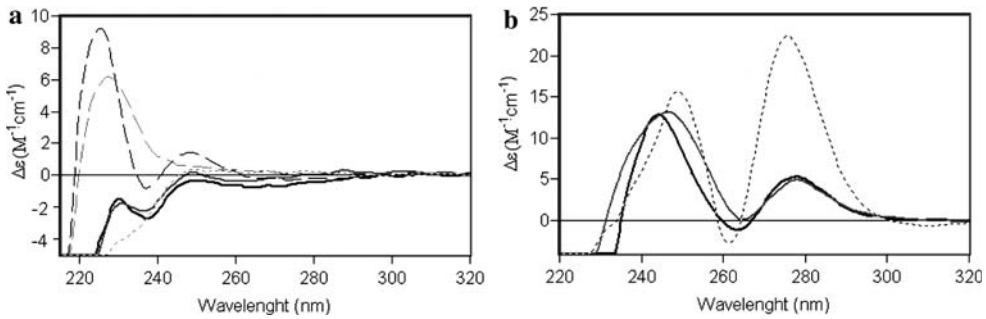

Fig. 10 **a** Comparison between the CD spectra of the mixture of equimolar amounts of Zn^{II}-N25 and Zn^{II}-C18 (*solid black line*) with the sum of the CD spectra of Zn^{II}-N25 and Zn^{II}-C18 (*solid grey line*). The CD spectra of Zn^{II}-N25 (*dotted line*), Zn^{II}-C18 (*dashed grey line*) and Zn^{II}-N25-C18 (*dashed black line*) are also included. **b** Comparison between the CD spectra of the mixture obtained in the cotitration of Zn^{II}-N25 and Zn^{II}-C18 after the addition of 7 equiv Cd^{II} (*solid black line*) and the sum of the final CD spectra of the separate titrations of Zn^{II}-N25 and Zn^{II}-C18 with Cd^{II} (*solid grey line*). The CD spectrum of recombinant Cd^{II}-N25-C18 (*dotted line*) is also included

which is definitely better than the parental strain at 2.5 and 3.5 μM Cd^{II} (Fig. 11b). This is highly consistent with the copper thionein character of the endogenous yeast MT, since we have shown that the single copy of *CUP1* present in the *cup1*^{S} strain is able to exhibit fairly normal growth under copper stress [32]. Cells synthesizing the QsMT-derived peptides exhibited a markedly reduced growth rate in relation to cells synthesizing QsMT. The higher the Cd^{II} concentration, the greater the disparity in growth rate between the pQsMT-transformed strain and the other three strains. This result is especially significant for N25-C18, which has the same number of Cys as QsMT and which yields aggregates of equivalent Cd^{II} and S^{2-} content (Table 2), with the only difference being the lack of the spacer region. This finding fully corroborates the same behaviour we previously reported for copper stress [32]. The obser-

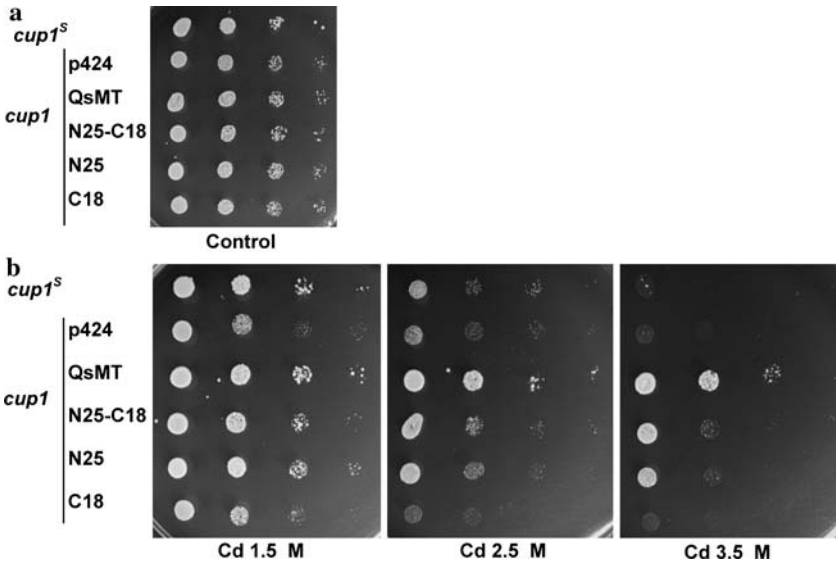

Fig. 11 Yeast functional complementation assays. The *cup1*^{S} strain presents only one copy of the *CUP1* gene, coding for an MT, while the *cup1*$^\Delta$ strain includes no copy of this gene. *cup1*$^\Delta$ cells have been transformed with the plasmid p424 without insertion, or with the constructions p424-QsMT, p424-N25-C18, p424-N25 or p424-C18. For the metal tolerance tests, transformed *cup1*$^\Delta$ cells were initially grown in selective SC-Trp-Ura medium and *cup1*^{S} strain in SC medium, both at 30 °C and 220 rpm to an optical density at 600 nm of 0.5–0.7. Cultures were then tenfold serially diluted three times, and 3 ml of each final sample was spotted on SC medium plates, supplemented or not supplemented with cadmium. Plates were incubated for 3 days at 30 °C and photographed. **a** Control SC medium without cadmium, to asses the viability of all the transformants. **b** The same medium supplemented with 1.5, 2.5 or 3.5 mM $CdCl_2$. The first column of each assay corresponds to the original culture, and each of the subsequent columns to its sequential tenfold dilution, as explained before

vation that the plant MT spacer is crucial for its in vivo metal detoxification function was already reported in [19] after comparison of the cadmium tolerance exhibited by yeast cells expressing different *Arabidopsis* MTs: MT1, an isoform naturally devoid of a spacer region, and MT2, an isoform with the typical plant MT sequence. The differences were then attributed either to the presence of the central domain or to the different arrangement of the Cys residues between both *Arabidopsis* MTs, but this second possibility can be now fully ruled out.

Conclusion

A comprehensive evaluation of all the data gathered provides a first approach to the structure/function relationship in a typical type 2 plant MT (QsMT) when coordinating Cd^{II}, which completes our previous studies of the Zn^{II}- and Cu^{I}-binding abilities of this same MT [30, 32]. For the sake of clarity, a synopsis of the stoichiometric and spectroscopic results is included (Scheme 2) with indication of the precise figure and/or table where they are shown.

All our current results are in full concordance with our previous assumption of rQsMT folding into a hairpin structure upon Zn^{II} coordination, enclosing four Zn^{II} ions and a low number of S^{2-} ligands, with no hint of participation of either the spacer region or, consequently, its His residue [32]. A hairpin model can now be also proposed for the in vivo folded Cd^{II}-rQsMT complexes. The ready dissimilarity between the rQsMT Cd^{II}-binding capacity and that deduced from the addition of those of N25 and C18 clearly rules out domain independence, thus discarding a dumbbell-like fold. Furthermore, the major species in the Cd^{II}-N25 and Cd^{II}-C18 preparations were dimeric Cd^{II} complexes, which further supports a hairpin model for Cd^{II}-rQsMT, as a dumbbell fold would rely on the ability of each Cys-rich region to fold into a monomeric metal complex. Consistently with the stoichiometric data, the CD analyses clearly reveal that the sum of Cd^{II}-N25 and Cd^{II}-C18 spectra is far from reproducing the CD fingerprint of any of the Cd^{II}-rQsMT types.

The unexpected recovery of distinct Cd^{II}-rQsMT types (Table 2) can be fully explained by assuming two alternative global conformations for the same hairpin fold. Hence, Cd^{II}-rQsMT(1) would be mainly composed of complexes containing six Cd(II) ions, with participation of four S^{2-} ligands but with no indication of the spacer His residue contribution. Conversely, Cd^{II}-rQsMT(3) would mainly consist of complexes of lower Cd^{II} content, (five Cd^{II}) and devoid of S^{2-} ligands, in which there are indications of Cd^{II}-His coordination, and therefore of the contribution of the spacer to the cluster architecture. This

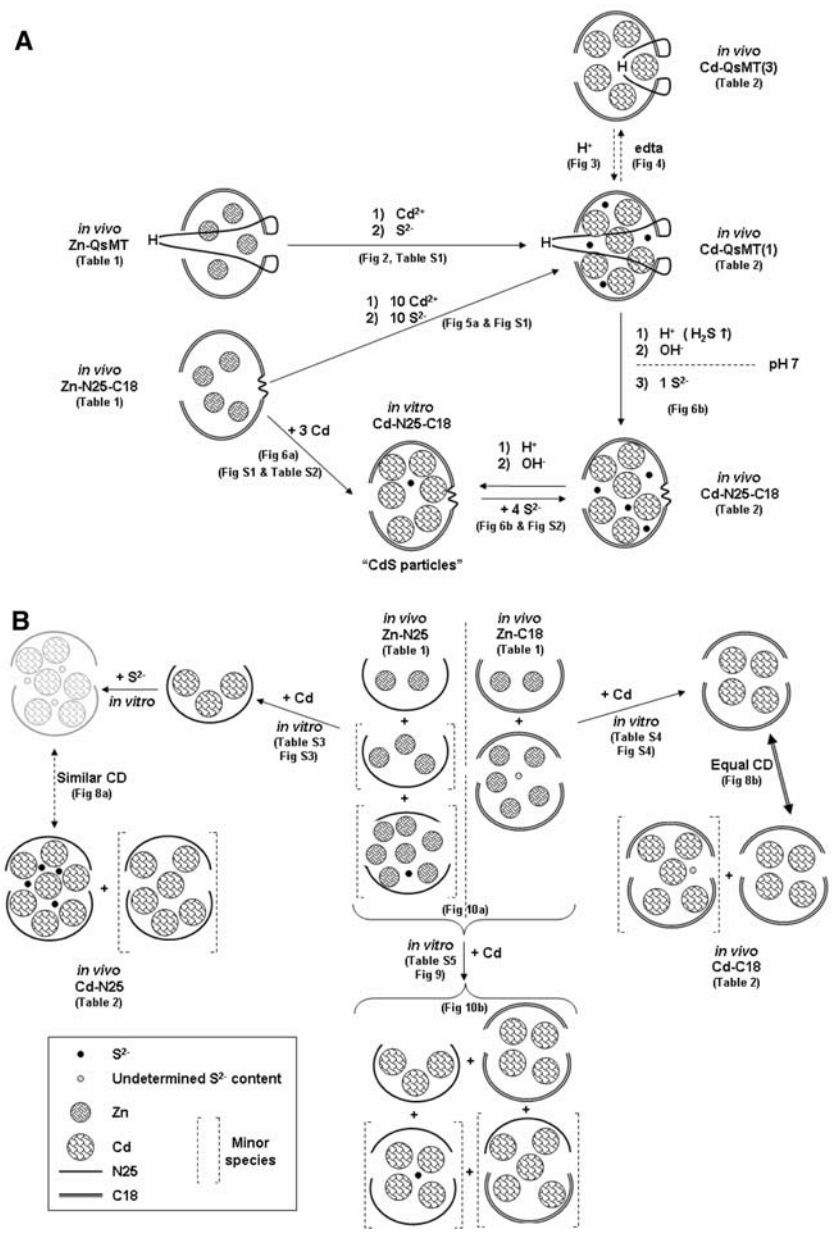

Scheme 2 The proposed composition and fold of the Zn^{II} and Cd^{II} complexes of recombinant **a** QsMT and N25-C18 and **b** N25 and C18. *In vivo* indicates a complex directly purified from recombinant synthesis, and *in vitro* refers to complexes obtained by the in vitro reaction indicated. For the sake of clarity the sulfide anions are shown reduced. When possible, the interrelationship between species has also been shown, as well as all the figures and tables from which the results have been drawn. The symbols used are detailed in the inset to *b*. H^+ sample acidification, OH^- sample reneutralization, S^{2-} sulfide addition, *grey* species of uncertain metal-to-protein stoichiometry, *dashed arrows* equivalences deduced from similar CD spectra

hypothesis is fully supported by the in vitro interconvertibility between both Cd^{II}-rQsMT types, inducible by slight acidification or demetalation treatments (Scheme 2a). Furthermore, it is also consistent with the facts that (1) complexes with at most five Cd^{II}, analogous to those of Cd^{II}-rQsMT(3), are obtained from the low-S^{2-}-containing Zn_4-rQsMT species by in vitro Zn^{II}/Cd^{II} replacement and (2) the subsequent addition of S^{2-} to the end of this titration renders species similar to those of Cd^{II}-rQsMT(1).

Following a similar reasoning to that used for rQsMT, our current data also suggest a hairpin model when N25-C18 binds Zn^{II} or Cd^{II} in vivo, although we rated this possibility as second best for Zn^{II}-N25-C18 in previous studies [32]. Cd^{II}-N25-C18 shares metal and sulfide content with Cd^{II}-rQsMT, but exhibits chirooptical properties different from those of all Cd^{II}-rQsMT types, which suggests that even if the spacer does not contribute to metal coordination, its presence determines some structural features that lead to different CD fingerprints for Cd^{II}-rQsMT(1) and Cd^{II}-N25-C18. This is exactly the same situation we observed for the Zn^{II}-binding features of these two polypeptides [32]. The lack of S^{2-} anions in the Zn^{II}-N25-C18 preparations also caused the Cd^{II}-N25-C18 complexes obtained from in vitro replacement to clearly differ from the in vivo recovered species, but again the spectroscopic features of both Cd^{II}-N25-C18 samples could

be mutually reproduced after the Acidification/reneutralization/sulfide-addition processes, this highlighting their close relationship (Scheme 2a).

Finally, the analysis of the separate N25 and C18 peptides provided further evidence for a hairpin folding model of Cd^{II}-rQsMT (Scheme 2b). C18, the smallest, six-Cys domain, yielded in vivo major monomeric complexes containing two Zn^{II}, but Cd^{II} coordination induced its dimerization both in vivo and in vitro, rendering Cd_4-$(C18)_2$ dimers. This tendency was already observed in Zn^{II} coordination by the presence of minor Zn_5-$(C18)_2$ forms, containing small amounts of S^{2-} (Table 1). Therefore, and probably owing to the cadmium ionic radius, formation of dimeric Cd^{II}-C18 complexes is favoured. The behaviour of N25 was more complex than that of C18, most likely because its greater length and higher Cys content enable it to alternate between monomers and dimers when binding Cd^{II}. In vivo, N25 basically folds into Zn_2 and Zn_3 monomers, although as for C18, the presence of minor S^{2-}-containing species already evidences a dimerization tendency. But, unlike C18, N25 gives completely different results for in vivo and in vitro Cd^{II} binding. Hence, in vivo, S^{2-}-containing Cd_7S_4-$(N25)_2$ or S^{2-}-devoid Cd_6-$(N25)_2$ dimers were recovered. This was in major concordance with the results for rQsMT and N25-C18, the two additional Cys in the N25 dimer easily accounting for the extra Cd^{II} bound (Cd_7S_4 and Cd_6 for dimeric N25, compared with Cd_6S_4 and Cd_5 for rQsMT and N25-C18). But in vitro, the Zn^{II}-N25 monomers evolve to Cd_3-N25 monomers, with once again subsequent S^{2-} addition at the end of this titration bringing the CD features of the sample close to those of the in vivo complexes. Therefore, the overall results of N25 analysis pointed to the tendency for dimerization being directly related to the availability of S^{2-} ligands, both conditions concomitantly enhancing the metal content of the clusters. If S^{2-} is absent or scarce, the dimeric Cd^{II} complexes are always a minor species. The result of the cotitration experiment further corroborates this hypothesis, both peptides behaving independently in low-sulfide conditions. In conclusion, if the tendency of both peptides is to dimerize when binding Cd^{II} in vivo, the most likely scenario is that N25-C18 and rQsMT fold into hairpin structures, to fully accomplish this requirement.

In summary, to our knowledge, this is the first characterization of type 2 plant MT Cd^{II}-binding behaviour, including a molecular dissection of its functional regions. Other studies were carried out with undigested fusion constructs and/or with other types of plant/algae MTs [23–27, 43]. We have shown that Cd^{II}-rQsMT most probably adopts a hairpin structure that increases its metal-binding capacity with the aid of S^{2-} ligands. The S^{2-}-devoid complexes always exhibit a lower Cd^{II} content and the data suggest that in this case the His residue from the spacer region most likely contributes to Cd^{II} coordination. The major participation of S^{2-} ligands in Cd^{II}-rQsMT complexes accounts for two uncommon features among MTs: the recovery of nonisostoichiometric Zn^{II} and Cd^{II} complexes, and the tendency for dimerization of the separate Cys-rich domains to enhance Cd^{II} coordination. Globally, all these attributes recall those of the well-known plant PCs, revealing similar molecular strategies of both Cys-rich polypeptides for Cd^{II} coordination.

Acknowledgements This work was supported by the Spanish Ministerio de Ciencia y Tecnología grants BIO2006-14420-C02-01 for S.A., BIO2006-14420-C02-02 for M.C. and AGL2003-00416 for M.M. G.M. and R.O. received predoctoral fellowships from the Pla de Formació de Personal Investigador del DURSI, Generalitat de Catalunya, and the Departament de Química, Universitat Autònoma de Barcelona, respectively. We especially want to acknowledge technical support from Roger Bofill and fruitful scientific discussions with Armida Torreggiani. We also thank the Serveis Científico-Tècnics de la Universitat de Barcelona (GC-FPD, ICP-AES, ESI-MS) and the Servei d'Anàlisi Química de la Universitat Autònoma de Barcelona (CD, UV–vis) for allocating instrument time.

References

1. Cobbett CS, Goldsbrough PB (2002) Annu Rev Plant Biol 53:159–182
2. Grill E, Winnacker E-L, Zenk M (1985) Science 230:674–676
3. Grill E, Winnacker E-L, Zenk M (1987) Proc Natl Acad Sci USA 84:439–443
4. Dameron CT, Winge DR (1990) Inorg Chem 29:1343–1348
5. Cobbett C, Goldsbrough P (2000) In: Raskin I, Ensley BD (eds) Phytoremediation of toxic metals: using plants to clean up the environment. Wiley, New York, pp 247–269
6. Reese RN, Wagner GJ (1987) Biochem J 241:641–647
7. Steffens JC, Hunt DF, Williams BG (1986) J Biol Chem 261:13879–13882
8. Rauser WE (2000) J Plant Physiol 156:545–551
9. Rauser WE, Curvetto NR (1980) Nature 287:563–564
10. Chatthai M, Kaukinen KH, Tranbarger TJ, Gupta PK, Misra S (1997) Plant Mol Biol 34:243–254
11. Morris CA, Nicolaus B, Sampson V, Harwood JL, Kille P (1999) Biochem J 338:553–560
12. Binz PA, Kägi JHR (2001) Metallothionein. http://www.bioc.uzh.ch/mtpage/MT.html
13. Robinson NJ, Tommey AM, Kuske C, Jackson PJ (1993) Biochem J 295:1–10
14. Murphy A, Taiz L (1995) Plant Physiol 109:945–954
15. van Hoof NA, Hassinen VH, Hakvoort HWJ, Ballintijn KF, Schat H, Verkleij JAC, Ernst WHG, Karenlampi SO, Tervahauta AI (2001) Plant Physiol 126:1519–1526
16. Guo W-J, Bundithya W, Goldsbrough PB (2003) New Phytol 159:369–381
17. Navabpour S, Morris K, Allen R, Harrison E, Mackerness SAH, Buchanan-Wollaston V (2003) J Exp Bot 54:2285–2292
18. Ma M, Lau P-S, Jia Y-T, Tsang W-K, Lam SKS, Tam NFY, Wong Y-S (2003) Plant Sci 164:51–60
19. Zhou J, Goldsbrough PB (1994) Plant Cell 6:875–884
20. Lee J, Shim D, Song W-Y, Hwang I, Lee Y (2004) Plant Mol Biol 54:805–815

21. Zimeri AM, Dhankher OP, McCaig B, Meagher RB (2005) Plant Mol Biol 58:839–855
22. Gonzalez-Duarte P (2003) In: McCleverty J, Meyer TJ (eds) Metallothioneins, comprehensive coordination chemistry II, vol. 8. Elsevier, Amsterdam, pp 213–228
23. Tommey AM, Shi J, Lindsay WP, Urwin PE, Robinson NJ (1991) FEBS Lett 292:48–52
24. Kille P, Winge DR, Harwood JL, Kay J (1991) FEBS Lett 295:171–175
25. Bilecen K, Ozturk UH, Duru AD, Sutlu T, Petoukhov MV, Svergun DI, Koch MHJ, Sezerman UO, Cakmak I, Sayers Z (2005) J Biol Chem 280:13701–13711
26. Peroza EA, Freisinger E (2007) J Biol Inorg Chem (in press). doi: 10.1007/s00775-006-0195-5
27. Freisinger E (2007) Inorg Chim Acta 360:369–380
28. Cols N, Romero-Isart N, Capdevila M, Oliva B, González-Duarte P, González-Duarte R, Atrian S (1997) J Inorg Biochem 68:157–166
29. Capdevila M, Cols N, Romero-Isart N, González-Duarte R, Atrian S, González-Duarte P (1997) Cel Mol Life Sci 53:681–688
30. Mir G, Domènech J, Huguet G, Guo WJ, Goldsbrough PB, Atrian S, Molinas M (2004) J Exp Bot 55:2483–2493
31. Capdevila M, Domènech J, Pagani A, Tío L, Villarreal L, Atrian S (2005) Angew Chem Int Ed Engl 44:4618–4622
32. Domènech J, Mir G, Huguet G, Capdevila M, Molinas M, Atrian S (2006) Biochimie 88:583–593
33. Bongers J, Walton CD, Richardson DE, Bell JU (1988) Anal Chem 60:2683–2686
34. Reese RN, Winge DR (1988) J Biol Chem 262:12832–12835
35. Gan T, Muñoz A, Shaw III CF, Petering DH (1995) J Biol Chem 270:5339–5345
36. Longo VD, Gralla EB, Valentine JS (1996) J Biol Chem 271:12275–12280
37. Mumberg D, Müller R, Funk M (1995) Gene 156:119–122
38. Domènech J, Tinti A, Capdevila M, Atrian S, Torreggiani A (2007) Biopolymers (in press). doi 10.1002/bip.20729
39. Maret W, Vallee BL (1993) Methods Enzymol 226:52–71
40. Lever ABP (1986) Inorganic electronic spectroscopy, 2nd edn. Elsevier, Amsterdam
41. Romero-Isart N, Cols N, Termansen MK, Gelpí JL, González-Duarte R, Atrian S, Capdevila M, González-Duarte P (1999) Eur J Biochem 259:519–527
42. Villarreal L, Tío L, Capdevila M, Atrian S (2006) FEBS J 273:523–535
43. Merrifield ME, Chaseley J, Kille P, Stillman MJ (2006) Chem Res Toxicol 19:365–375